



# Experimental study of mechanical properties of artificial dam for coal mine underground reservoir under cyclic loading and unloading

Xin Lyu · Ke Yang · Chaoshui Xu · Juejing Fang ·  
Minke Duan · Zhainan Zhang

Received: 20 July 2023 / Accepted: 9 May 2024  
© The Author(s) 2024

**Abstract** This study investigates the stability of an artificial dam used in an underground reservoir in a coal mine under periodic weighting imposed by overlying rock strata. For this purpose, cyclic loading and unloading tests with different stress amplitudes were designed. Differences in the mechanical performance of the artificial dam with and without overlying strata were analyzed using a uniaxial compression test. The mechanical properties of the structure under constant-amplitude cyclic loading and unloading were characterized. Further, the law of influence of stress amplitude on stability was discussed. A formula for predicting the mechanical performance of the artificial dam with its overlying rocks (hereafter referred to as the complex) was finally derived and was suitable

for clarifying the law of damage in the complex under cyclic loading and unloading. The results showed that the complex had changed the internal structure of rocks. The strength and deformation of the complex were intermediate to that of either single structure. All three underwent brittle failure. During the constant-amplitude loading and unloading tests, the hysteresis loop could be divided into three phases, namely, sparse, dense, and sparse again, with a shift in the turning point in rock deformation memory effect. As the stress amplitude increased during the test, the damping ratio of the specimens decreased, and the area of the hysteresis loop increased non-linearly. The dynamic elastic modulus decreased first and then increased. The confidence interval for the formula fitted based on the test results was above 97%. Damage to the complex caused by constant-amplitude loading and unloading could be divided into three stages. An increase in peak stress served as a catalyst for the evolution of small cracks within the specimens into median and large cracks, thereby accelerating the damage process.

---

X. Lyu · J. Fang · Z. Zhang  
State Key Laboratory of Mining Response and Disaster  
Prevention and Control in Deep Coal Mines, Anhui  
University of Science and Technology, Huainan, China

X. Lyu · C. Xu  
School of Civil, Environmental and Mining Engineering,  
The University of Adelaide, Adelaide, Australia

Ke. Yang (✉)  
Institute of Energy, Hefei Comprehensive National Science  
Center, Hefei, Anhui, China  
e-mail: keyang2003@163.com

M. Duan  
Anhui Provincial Closed/Abandoned Mine Resource  
Development and Utilization Engineering Research  
Center, Huainan, China

## Article highlights

- To study the mechanical properties of constant-amplitude cyclic loading and unloading of artificial dam assemblies in abandoned mine reservoirs.

- Summarize the law of cyclic loading and unloading characteristics, and obtain the performance prediction formula of composite structure.
- Explore the damage mechanism of equal-amplitude cyclic loading and unloading, and monitor the internal pore changes.

**Keywords** Abandoned mines · Underground reservoir · Artificial dam complex · Stress amplitude · Constant-amplitude loading and unloading · Nuclear magnetic resonance

## 1 Introduction

China has been making unremitting efforts to achieve carbon peak and carbon neutrality goals and to cut overcapacity, radically changing China's energy consumption structure. However, the number of abandoned coal mines in China has been increasing every year (Lyu et al. 2022, 2023a). Utilization of abandoned coal mines has become the best pathway for coal enterprises to transform themselves and achieve low-carbon development. Building underground pumped storage power stations have proved feasible for exploiting residual underground spaces and water resources, generating renewable energy (e.g., wind and solar energies) (Chelidze et al. 2019; Lyu et al. 2023c; Ghosh et al. 2022), and peak-shaving and valley-filling the power consumption profile, thereby bringing huge economic benefits for enterprises.

Artificial dams are critical parts of underground reservoirs. Stability of the artificial dam complex is a top priority and has been intensively and extensively studied (Chen et al. 2023; Li et al. 2022; Yang et al. 2022a, b, c). Typical studies usually cover the following aspects: the manner in which man-made structures are embedded in original coal rocks, reserved width of the dam (Liu et al. 2023; Ma et al. 2023a, b, c), and properties of different coal rocks are considered when using theoretical and experimental approaches to compare the stress transfer in dam complexes and analyze the dynamic stress–strain relationship (Fang et al., 2022; Nie et al. 2023), instability, and failure characteristics for the complexes (Ren et al. 2022; Wang et al. 2023a, b, c, d; Lu et al. 2023); an angle is preset to determine the influence of formation dip on the load-carrying properties of the complex so as

to understand the interface weakening mechanism; acoustic emission technique may be employed to determine the energy dissipation law in the complex (Ma et al. 2023a, b, c; Meng et al. 2023b; Song et al. 2023).

The greatest difference between an underground structure and an aboveground structure lies in the disturbance caused by overlying rocks. Overlying rocks not only exert enormous loads on underground structures, but also induce periodic weighting. Cyclic and reciprocating external forces (Meng et al. 2023a; Tang et al. 2022; Zhou et al. 2023), including earthquakes, detonation, and mechanical vibrations, have been simulated by cyclic loading and unloading schemes (Zheng et al. 2023; Yang et al. 2023; Xue et al. 2021; Maddu et al. 2022). Using this method, the influence of the cyclic loading frequency on the fatigue life of rock formations is studied, and the differences across lithologies are quantified (Wang et al. 2023a, b, c, d; Ma et al. 2023a, b, c; Liu et al. 2020; Yang et al. 2019). The failure characteristics of rocks under different confining pressures during cyclic loading and unloading are investigated, and the damage and failure process of the specimens is revealed from the perspective of energy dissipation (Zhang et al. 2023a, b, c). In this way, researchers can obtain the physical and mechanical features of rock specimens subjected to constant-amplitude cyclic loading and unloading, including the compressive strength (Zhang et al. 2023a, b, c; Wang et al. 2021), deformation parameters, and shear parameters. The influence of cyclic loading and unloading on the motion pattern of mineral particles is usually characterized by microstructural observation. A damage constitutive model of rock specimens can be built based on the above (Zhang et al. 2023a, b, c; Wang et al. 2023a, b, c, d; Li et al. 2023).

The use of artificial dams for coal mine underground reservoirs has already drawn widespread attention. However, most relevant studies are related to the mechanical performance of coal-rock assemblages. Besides, incremental loading and unloading, which is commonly used in coal mine production, is chosen as the preferred test scheme. We still know little about the combined bearing capacity of an artificial dam with overlying rocks when associated with abandoned coal mines, especially when subjected to constant-amplitude cyclic loads exerted by the overlying rocks.

In this study, an artificial dam with overlying rocks (hereafter referred to as a complex) used with a reservoir in an abandoned coal mine was subjected to constant-amplitude cyclic loading and unloading under different stress amplitudes. X-ray diffraction analysis (XRD) and nuclear magnetic resonance (NMR) were employed to detect the differences in composition and internal structure of the artificial dam and its overlying rocks. A uniaxial compression test was performed to obtain the strength and deformation laws of the complex. The constant-amplitude cyclic loading and unloading curves were analyzed. The hysteresis loop was divided into three phases, and the features for each phase were determined. We also obtained the damping ratio, dynamic elastic modulus, and the variation trend of the area of the hysteresis loop for the complex. A theoretical formula with a high confidence level was fitted for predicting damage development in the complex under cyclic loading and unloading. Our research findings provide theoretical and experimental clues for long-term stability assessment of underground reservoirs.

## 2 Specimens of artificial dam complex and the loading–unloading scheme

### 2.1 Experimental materials

The complex specimen consisted of two parts. Specimens were prepared using natural rocks and by pouring concrete to ensure the accuracy of tests.

First, samples of massive red sandstone formations were collected from the Xiegou Coal Mine and made into a  $\Phi 50 \text{ mm} \times L50 \text{ mm}$  cylinder using a core drilling machine. After processing, the rock specimen was placed at the bottom of a  $\Phi 50 \text{ mm} \times L100 \text{ mm}$  cylindrical mold. Next, cement and water were mixed in a mass ratio of 3:1. Finally, the slurry was poured into the mold and subjected to homogenization and oscillation.

The specimen was demolded after curing for 24 h and then placed in a naturally ventilated room for 28 d. Subsequently, rough edges were trimmed away from the two end faces by fine sanding. The unevenness of the two end faces did not exceed 0.05 mm, and the non-perpendicularity of any two adjacent faces did not exceed  $\pm 0.5^\circ$  (Fig. 1).

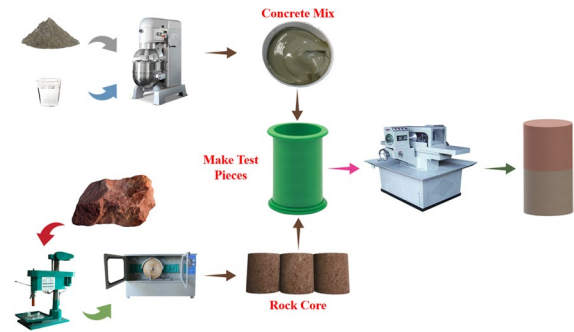


**Fig. 1** Preparation of artificial dam specimen

Eight groups of specimens were designed for tests. Three groups were used for uniaxial compression tests, namely, red sandstone specimens (simply known as Rock), artificial dam specimens (simply known as Dam), and complex specimens (simply known as DR). The remaining five groups were used for the cyclic loading and unloading tests, and all of them were DR.

XRD was performed for the Rock and DR specimens (Fig. 2). As shown by the analysis, the red sandstone specimens had the highest quartz content of 70.9%. The complex specimens were more uniform in composition, and the hydration reaction products were the predominant components.

### 2.2 Test scheme and key technical measures

RMT-150B rock mechanics test system was used for the loading tests (Fig. 3). Two modes of tests were configured, namely, uniaxial compression test and cyclic loading and unloading test.

#### (1) Uniaxial compression test.

The specimen was placed on the lower pressing plate of the test system, its center being aligned with the center of the lower pressing plate. A digital dial gauge was installed and connected to a computer for debugging.

The loading rate was set to 1 kN/s, and the displacement acquisition frequency was 100 ms. An axial stress was imposed by the test system until the specimens finally failed. The test data were acquired, recorded, saved, and processed (Fig. 4).

#### (2) Cyclic loading and unloading test.

Based on the uniaxial compressive strength of the complex specimens, the initial load imposed on the

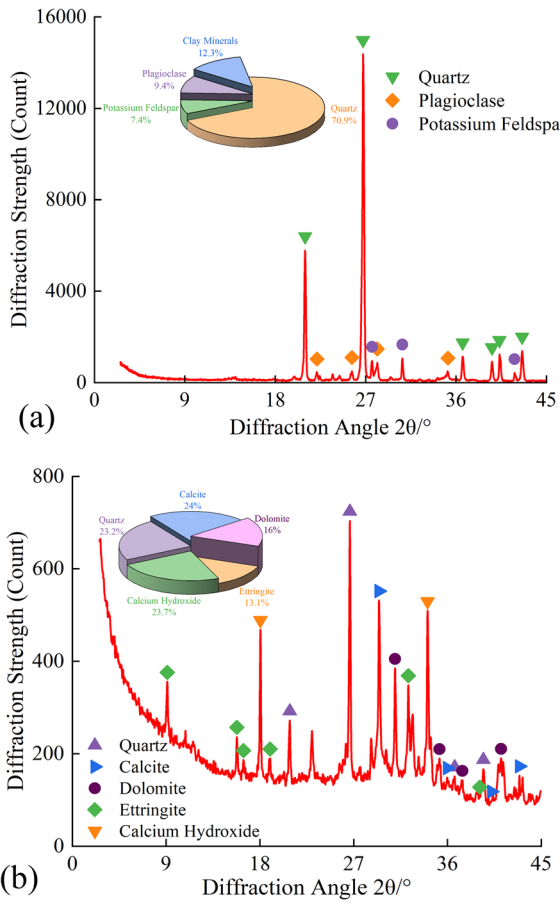


**Fig. 2** X-ray diffraction patterns: **a** X-ray diffraction pattern of red sandstone; **b** X-ray diffraction pattern of artificial dam

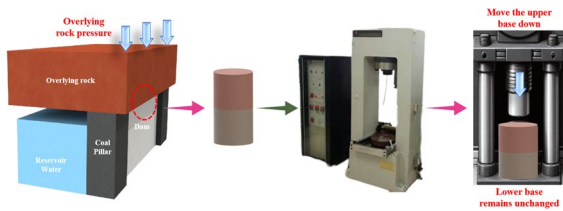


**Fig. 3** Loading method

complex specimens was set to 4 MPa. The stress gradient was 4 MPa between two adjacent groups. That is, the stress amplitudes for different groups were 4 MPa, 8 MPa, 12 MPa, 16 MPa, and 20 MPa, successively. The constant-amplitude load was applied for 30 cycles (Fig. 5).

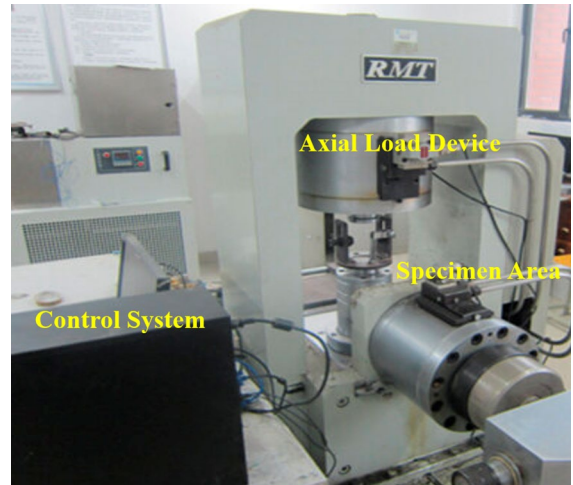


**Fig. 4** Test equipment

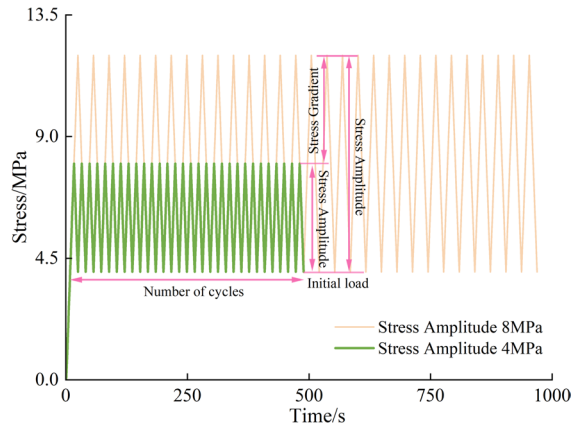


**Fig. 5** Loading and unloading scheme

The loading and unloading rates were set to 1 kN/s. The loading and unloading scheme was integrated with the control program. Automatic control was applied using the axial loading device of the test system, and the data were saved in real-time.

### 3 Test results and analysis for the complex

#### 3.1 Test results and analysis for the complex

During axial loading, the base of the test system remained immobile, while the upper portion descended. For this reason, rocks were placed above

the artificial dam to form the complex to simulate the pressure exerted by overlying rocks on the dam.

Stress–strain curves and other data were obtained from tests for each group of specimens (Table 1 and Fig. 6). Representative data were chosen for each group and plotted in the graphs.

It can be seen from Fig. 6 that the full stress–strain curves were divided into five phases, namely, compaction of original voids, linear elasticity, transition from elastic to plastic phase, plasticity, and failure. After the specimens reached peak strength, the stress dropped rapidly, which was typical of brittle failure. The features of each phase varied for the different specimens. The compaction stage was the longest with red sandstone specimens, followed by the artificial dam specimens and complex specimens, respectively. This is because natural rocks are rich in pores and cracks and take longer to be compacted at the early stages of loading. On the contrary, artificial structures are denser and more uniform. The slurry invaded the red sandstone during the preparation of the complex specimens, which changed the internal structure of the complex (Yang et al. 2022b; Lyu et al. 2023b). Moreover, the structure of half rock and half artificial structure makes the overall porosity of the specimen be between the two monomers, so the artificial dam combined specimen takes into account the characteristics of both.

The compressive strength and axial strain of the complex were intermediate between those of either the red sandstone or the artificial dam (Fig. 7). Compared with red sandstone, the complex had compressive strength and strain that decreased by 31.00% and 24.90%, respectively. Meanwhile, compared with the

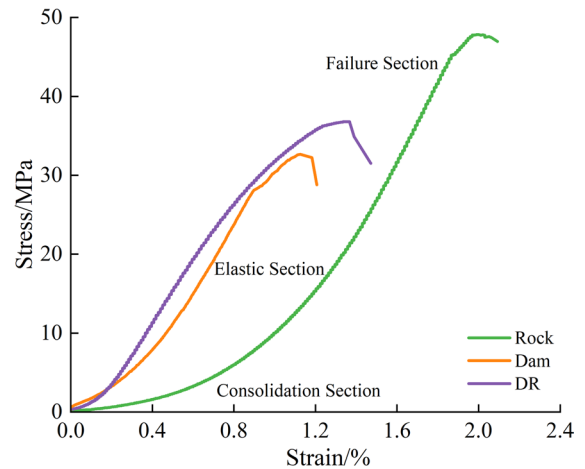


**Fig. 6** Stress–strain curves of the specimens

artificial dam, the complex had compressive strength and strain that increased by 12.91% and 10.23%, respectively. Although the increase and the decrease were of similar amplitude, the compressive strength varied more significantly, indicating that the interface between the two media influences the strength to a great extent (Yang et al. 2022c).

### 3.2 Loading and unloading curves of the complex

A typical complex specimen was chosen for plotting the cyclic loading and unloading stress–strain curve (Fig. 8). During the 30 loading and unloading cycles, variation in the length of the curve segment for each cycle was divided into three phases, namely, sparse,

**Table 1** Test results

No	Stress/MPa	Strain/%	Mean stress/MPa	Mean strain/%
Rock-A	47.82	1.99	48.14	1.92
Rock-B	49.51	2.04		
Rock-C	47.10	1.73		
Dam-A	34.56	1.11	32.80	1.17
Dam-B	33.34	1.13		
Dam-C	30.50	1.28		
DR-A	34.80	1.23	36.15	1.32
DR-B	36.81	1.35		
DR-C	36.85	1.36		

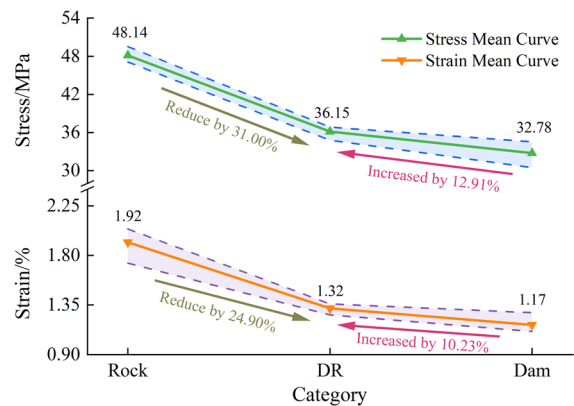


**Fig. 7** Mean stresses and strains



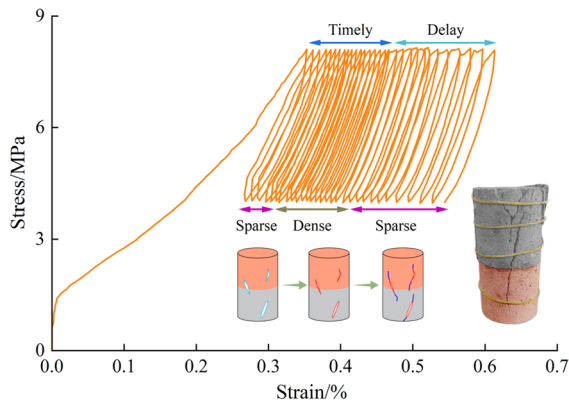


**Fig. 8** Loading and unloading curves of specimens

dense, and sparse. Pores and cracks were closed in the specimens at the initial loading stage. Therefore, the loading curve displayed a hysteresis effect. The specimens became more compacted in the middle of loading, and the resistance to deformation also increased. The load response was faster at this stage. Later, more cracks were developed within the specimens, increasing the deformation. Meanwhile, progressive hysteresis was observed for the peaks in each cycle. Cracks and fractures within the specimens led to fluctuations in the stress–strain curves.

As a composite structure, the artificial dam complex contained some native defects along with an artificial interface and hence, served as a typical non-ideal elastoplastic body. Under cyclic loading and unloading, the dynamic stress and dynamic strain curves for the artificial dam complex would not be synchronized as in the case of an ideal elastoplastic body. During the cyclic loading and unloading process, recoverable elastic deformation and unrecoverable plastic deformation existed simultaneously, and the stress–strain curves formed a hysteresis loop. The hysteresis curve shifted continuously towards the right as cyclic loading and unloading proceeded. Repeated alternation of the upper and lower load limits accelerated the plastic deformation rate for the artificial dam complex, which further increased the area of the hysteresis loop.

Rocks and metals have the capacity to record the external influences acting on themselves and exhibit the features of such influences via some physical quantities. These phenomena are known as memory effects, among which deformation memory effect is

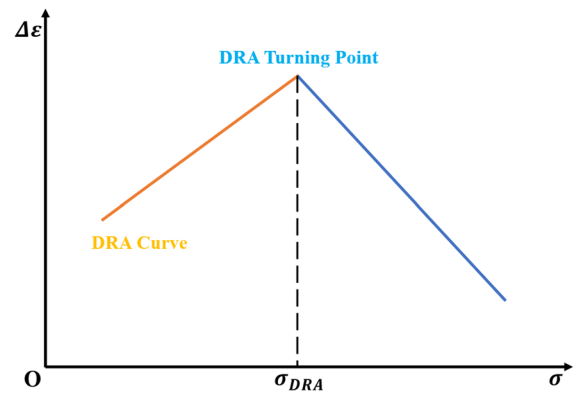


**Fig. 9** DRA curve

one. Retrieving this recorded information by analyzing rock deformation data from the attributes of the rock has proven feasible. Deformation rate analysis (DRA) utilizes the deformation memory effect. As shown in Fig. 9, the strain difference as a function  $\Delta\varepsilon_{i,j}(\sigma)$  is written as follows:

$$\Delta\varepsilon_{i,j}(\sigma) = \varepsilon_j(\sigma) - \varepsilon_i(\sigma) \quad (j > i) \quad (1)$$

where  $\varepsilon_i(\sigma)$  and  $\varepsilon_j(\sigma)$  are the axial strains in the  $i$ th and  $j$ th loading cycles, respectively;  $\sigma$  is the corresponding axial stress. Compressive stress and compressive strains were defined as positive. In Eq. (1), the reversible strain components of the axial strain curve in two consecutive compression cycles were removed to obtain the difference in axial non-reversible strain  $\Delta\varepsilon$ .

The loading stage of the fifteenth cycle of each artificial dam composite specimen was selected as the measurement stage to calculate the DRA curve. An average was taken for specimens subjected to constant-amplitude loading and unloading tests under the same stress amplitude (Fig. 10). As the same material is used to prepare the complex specimens, the DRA curves shared a similar trend for different stress amplitudes in the loading and unloading tests. Nevertheless, as the stress amplitude changed, the rock deformation memory effect in the complex specimens also varied. Damage accumulation in the specimens varied with peak stress. The crack size changed under different stress amplitudes, and the cracks developed and evolved within the specimens, changing the rock deformation memory. Under the same gradient, as the stress amplitude increased (from 4 to 20 MPa),

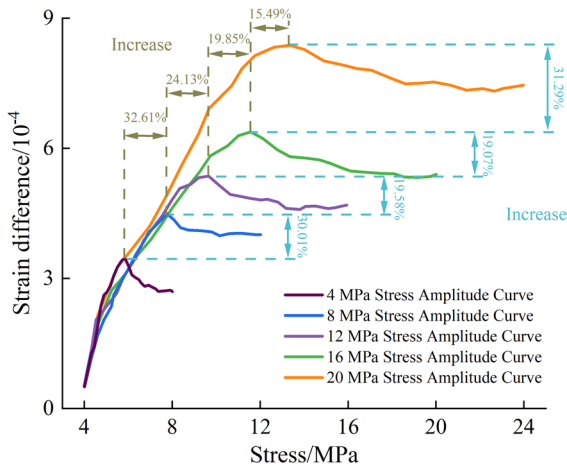


**Fig. 10** DRA curves of specimens

the resulting change rate at the turning point gradually decreased from 32.61% to 15.49%, indicating the presence of a limit value for the turning point.

### 3.3 Results from cyclic loading and unloading tests in complex specimens

Since the artificial dam complex is not a non-ideal elastoplastic body, there would be a lag between the dynamic stress and dynamic strain during cyclic loading and unloading tests under different stress amplitudes. Thus, the load-deformation curves make a hysteresis loop (Fig. 11), which is indicative of the distinct features of structural deformation under repeated loading. Irreversible damage occurred within the specimens, indicating that energy was dissipated within the specimens.

The dynamic elastic modulus  $E_d$  and the damping ratio  $\lambda$  are respectively defined as follows:

$$E_d = \frac{\sigma_{max} - \sigma_{min}}{\epsilon_{max} - \epsilon_{min}} \tag{2}$$

$$\lambda = \frac{A}{4\pi A_s} \tag{3}$$

where  $A$  is the area of the hysteresis loop ABCDA;  $A_s$  is the area of the triangle AEF.

For each specimen, hysteresis data of the fifteenth cycle were chosen for analysis. An average was taken for each group of complex specimens.

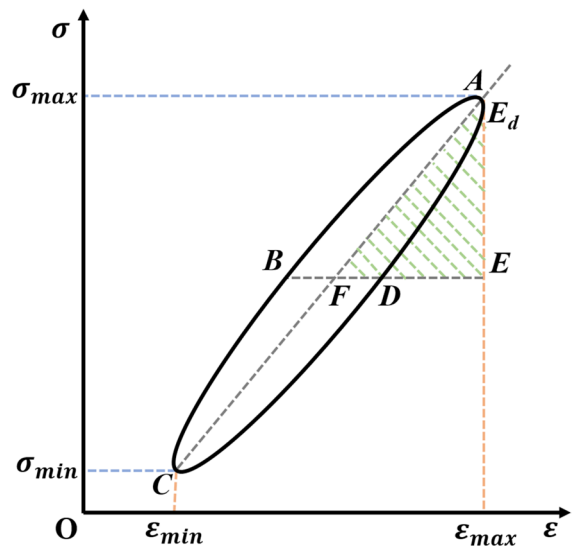


**Fig. 11** Hysteresis loop of dynamic stress and dynamic strain

As shown in Fig. 12, as the stress amplitude increased in the cyclic loading and unloading tests (from 4 to 20 MPa), the damping ratio decreased consistently. The decrease rate dropped over time as well, from 50.79% to 42.86%, 25.00%, and 17.89%, respectively. Damping ratio is a measure of dissipated energy within specimens. In our tests, the damping ratio decreased as the stress amplitude increased. This result indicated that under a high stress amplitude, energy was mostly dissipated through plastic deformation induced by crack propagation and penetration

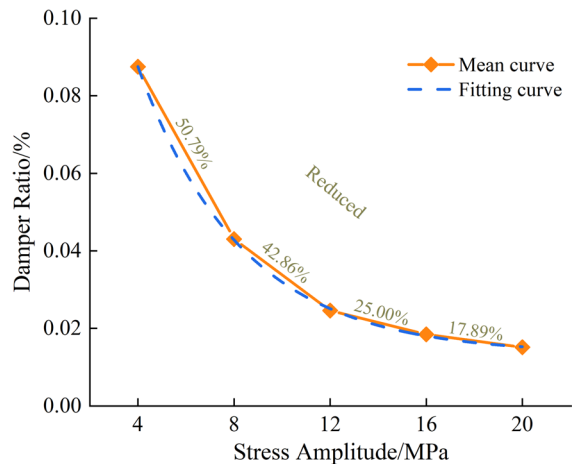


**Fig. 12** Damping ratio of DR

on the macroscopic scale. By contrast, under a low stress amplitude, energy was mostly dissipated through the generation of microcracks, and a greater portion of energy was dissipated by inducing internal damage of the specimens.

The relationship between the stress amplitude of cyclic loading and unloading and the damping ratio of the complex specimen was fitted, as below:

$$\lambda = 0.0134 + 0.1867e^{-\frac{\sigma_x}{4.3284}} \tag{4}$$

where  $\sigma_x$  is the stress amplitude of cyclic loading and unloading, MPa. The correlation coefficient  $R^2=0.9998$ , indicating good non-linear relationship between the stress amplitude and damping ratio of the artificial dam complex. This fitting formula is suitable for predictions for the same materials.

As shown in Fig. 13, as the stress amplitude of cyclic loading and unloading increased, the dynamic elastic modulus first decreased and then increased for the artificial dam complex. Besides, the decrease in the amplitude was far greater than the increase in the amplitude. This is because at a smaller stress amplitude, the compaction stage lasted longer and accounted for a larger proportion of the hysteresis loop. Therefore, changing the lower stress limit resulted in a higher value of dynamic elastic modulus than the real value of the material. As the stress amplitude continued to increase, compaction accounted for a decreasing proportion of the

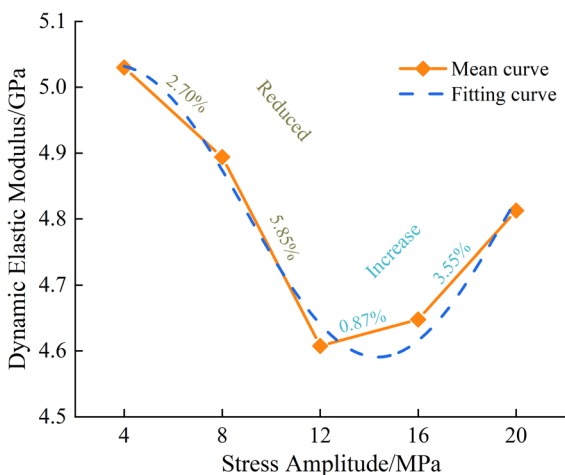


**Fig. 13** Dynamic elastic modulus of the artificial dam complex

hysteresis loop made up of stress–strain curves, with a stabilization of numerical values. Meanwhile, a high stress amplitude tended to make the specimens more homogenous, and the dynamic elastic modulus increased as well.

The dynamic elastic modulus was fitted for complex specimens under different stress amplitudes. Thus, we obtained

$$E_d = 4.8120 + 0.2213 \sin\left(\pi \frac{\sigma_x + 1.7882}{10.7580}\right) \tag{5}$$

The correlation coefficient  $R^2=0.9771$ , indicating the feasibility of using the above fitted formula to predict the dynamic elastic modulus under a specific stress amplitude.

As the stress amplitude of cyclic loading increased for artificial dam specimens, the area of the hysteresis loop also increased continuously (Fig. 14), signifying an increase in the damage within the specimens. Our results indicated that as the stress amplitude increased, the damage in the specimens increased as well. At a low stress amplitude, the cyclic loading and unloading tended to close the original cracks in the specimens, though there was little impact on crack growth and development. The specimens were compacted as the pores and cracks were closed with increasing stress amplitude. The compaction stage was followed by the elastic deformation stage, during which regenerative cracks appeared, and the damage continued to grow. However, the increase rate of the

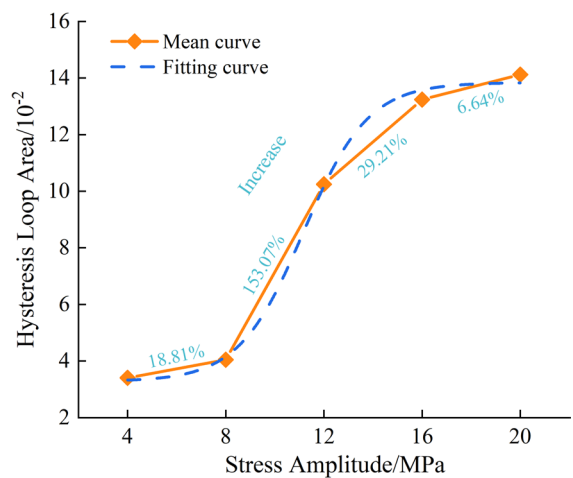


**Fig. 14** Area of hysteresis loop for the complex



damage was lower at the elastic stage, and due to the limited increase in stress amplitude, the quantitative changes did not become qualitative yet.

The area of the hysteresis loop for the artificial dam complex was fitted and the expression was obtained as

$$A = 13.8396 - \frac{10.5603}{1 + e^{\frac{\sigma_x - 11.1652}{1.3179}}} \quad (6)$$

The correlation coefficient  $R^2 = 0.9978$ , indicating the feasibility of using the fitted formula to predict the mechanical performance of the artificial dam complex during the compaction stage and elastic deformation stage under cyclic loading and unloading.

#### 4 Damage analysis of the complex

Existing studies have shown that the ultimate deformation of specimens subjected to cyclic loading and unloading at a specific stress amplitude is free from the influence of the stress amplitude and loading frequency and remains relatively stable (Wang et al. 2023a, b, c, d). Therefore, the maximum strain was treated as the damage variable. The damage accumulation and failure criteria were stable and independent of loading conditions. The damage variable was defined as follows:

$$D = \frac{\epsilon_{\max}^n - \epsilon_{\max}^0}{\epsilon_{\max}^f - \epsilon_{\max}^0} \quad (7)$$

where  $\epsilon_{\max}^0$  is the strain peak during the first loading–unloading cycle;  $\epsilon_{\max}^n$  is the strain peak during the  $n$ th loading–unloading cycle;  $\epsilon_{\max}^f$  is the peak strain when the specimen fails.

The damage variation curve could be divided into three stages (Fig. 15). The interface was compacted and the pores and cracks were compressed in specimens subjected to a smaller number of cycles. At this stage, the specimens underwent significant deformation, and the value of the damage variable rose steeply. As the number of cycles increased, the specimens underwent elastic deformation. The elastic deformation stage lasted longer, but the deformation was minor, albeit with a steady increase in damage. As the number of cycles increased, the initiation of regenerative cracks in the specimens began. Crack

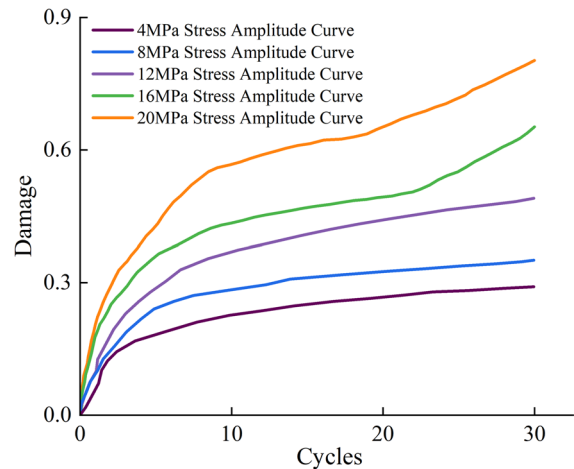


Fig. 15 Curves of damage vs. cycles

propagation and coalescence occurred, and the damage variable increased sharply.

At a low stress amplitude, the compaction stage of the specimens had not yet been completed, and the initial increase in damage was small. The steady increase stage seemed to last for a longer period of time. But at a higher stress amplitude, the compaction stage came to an end at a higher speed, resulting in irreversible deformation. After the elastic deformation stage, the damage growth in the specimens accelerated. But due to the limited number of cycles, complete damage did not occur ( $D = 1$ ).

NMR was performed for complex specimens using the Micro MR Series NMR Analyzer after cyclic loading and unloading. NMR scan was performed at saturation by taking a sample at approximately 2 mm from the interface at the center. The spin–spin relaxation time ( $T_2$ ) changes of the water molecules were utilized to characterize the pore structure.

Four types of pores were defined based on pore size in the pore size distribution graph (Fig. 16): micropores (0–0.001  $\mu\text{m}$ ), small pores (0.001–0.1  $\mu\text{m}$ ), mesopores (0.1–10  $\mu\text{m}$ ), and large pores (> 10  $\mu\text{m}$ ).

At a low stress amplitude, the original pores and cracks in the specimens were compressed, but there were still residues. As the stress amplitude increased, the wave peaks decreased in both small pores and mesopores. Besides, the decrease of amplitude in small pores was larger than that in mesopores, while the large pores were not yet developed. At a higher stress amplitude, secondary cracks were developed

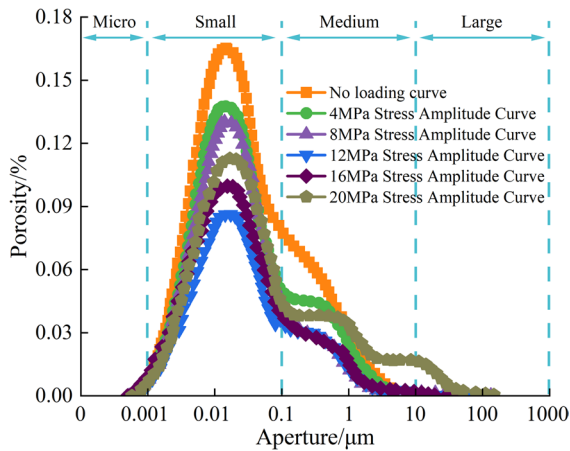


**Fig. 16** Pore size distribution of the artificial dam complex

in the specimens, and the number of each type of pores increased significantly. However, small pores and mesopores still dominated, while large pores did not entirely penetrate the specimens, leading to instability.

## 5 Conclusion

The main conclusions of this study are as follows:

- (1) Natural rocks differ significantly from artificial structures in composition. Under uniaxial compressive loading, red sandstone and artificial dams with or without overlying rocks underwent brittle failure predominantly. Besides, the strength and deformation of the complex were intermediate to the single structures.
- (2) During constant-amplitude cyclic loading and unloading, the hysteresis loop for the complex was divided into three phases, namely, sparse, dense, and sparse again. The area of the hysteresis loop gradually increased, and the rock deformation memory curves shared similar trends. However, as the stress amplitude increased, the turning point shifted towards the right.
- (3) As the stress amplitude of cyclic loading and unloading increased, the damping ratio increased, and the area of the hysteresis loop increased nonlinearly before finally stabilizing. For the artificial dam complex, the dynamic elastic modulus first decreased and then increased. A formula was

then fitted to predict the mechanical performance of the complex.

- (4) Damage to the complex caused by constant-amplitude loading and unloading could be divided into three stages. An increase in stress amplitude accelerated the damage process of specimens and changed the pore size distribution, promoting the growth of small cracks into medium and large ones.

**Acknowledgements** Our deepest gratitude editors and anonymous reviewers of serious work and thoughtful recommendations that greatly improve the paper. Thank you for the financial support provided by the China Scholarship Council Fund [No.: 202208340045], the Regional Innovation and Development Joint Fund of National Natural Science Foundation of China [No.: U21A20110] and the Open Project Program of Anhui Engineering Research Center of Exploitation and Utilization of Closed/abandoned Mine Resources [No.: EUCMR202201], thanks to Hefei Comprehensive National Science Center [No.: 21KZS215] for help. The authors were grateful for the great support awarded.

**Author contributions** Each author has contributed to this work. XL and JF conceived and designed the experimental scheme; XL and ZZ performed the experiment; XL and MD processed the experimental data and wrote this paper; KY and CX improved the paper's structure and language. All authors read and approved the final manuscript.

**Funding** This work was funded by the China Scholarship Council Fund [No.: 202208340045], the Regional Innovation and Development Joint Fund of National Natural Science Foundation of China [No.: U21A20110], the Open Project Program of Anhui Engineering Research Center of Exploitation Fund [No.: EUCMR202201] and Hefei Comprehensive National Science Center [No.: 21KZS215].

**Data availability** The data that support the findings of this study are available from the corresponding author, upon reasonable request.

### Declarations

**Conflict of interest** The authors declare that they have no known competing financial interests or personal relationships that could have appeared to influence the work reported in this paper.

**Ethical approval** Not applicable.

**Consent for publication** The authors confirm that this work has not been published before, and its publication has been approved by all co-authors.

**Open Access** This article is licensed under a Creative Commons Attribution 4.0 International License, which permits use, sharing, adaptation, distribution and reproduction in any medium or format, as long as you give appropriate credit to the original author(s) and the source, provide a link to the Creative Commons licence, and indicate if changes were made. The images or other third party material in this article are included in the article's Creative Commons licence, unless indicated otherwise in a credit line to the material. If material is not included in the article's Creative Commons licence and your intended use is not permitted by statutory regulation or exceeds the permitted use, you will need to obtain permission directly from the copyright holder. To view a copy of this licence, visit <http://creativecommons.org/licenses/by/4.0/>.

## References

- Chelidze T, Matcharashvili T, Abashidze V, Tsaguria T, Dvagal N, Zhukova N (2019) Complex dynamics of fault zone deformation under large dam at various time scales. *Geomech Geophys Geo* 5(4):437–455
- Chen YL, Hao XJ, Xue DJ, Li Z, Ma XR (2023) Creep behavior and permeability evolution of coal pillar dam for underground water reservoir. *Int J Coal Sci Technol*. <https://doi.org/10.1007/s40789-023-00563-y>
- Fang JJ, Yang K, Lyu X, Tang JZ, Zhang JQ (2022) Mechanical properties and instability analysis of concrete specimens with horizontal holes of different diameters. *Front Earth Sci*. <https://doi.org/10.3389/feart.2022.949043>
- Ghosh T, Gujjala YK, Deb D, Sekhar GPR (2022) Numerical investigation of spontaneous imbibition in an anisotropic reservoir. *Geomech Geophys Geo*. <https://doi.org/10.1007/s40948-022-00411-4>
- Li N, Xie HP, Hu JJ, Li CB (2022) A critical review of the experimental and theoretical research on cyclic hydraulic fracturing for geothermal reservoir stimulation. *Geomech Geophys Geo*. <https://doi.org/10.1007/s40948-021-00309-7>
- Li X, Zhang H, Wu D, Guo Y, Ren K, Tan Y (2023) Strength deterioration characteristics of lime-metakaolin improved earthen site soil under freeze-thaw cycles. *Rock Soil Mech* 44(6):1593–1603
- Liu C, Yu BC, Zhang DM, Zhao HG (2020) Experimental study on strain behavior and permeability evolution of sandstone under constant amplitude cyclic loading-unloading. *Energy Sci Eng* 8(2):452–465
- Liu SJ, Wang ZQ, Kou MM, Zhang YJ, Wang YL (2023) Phase-field simulations of unloading failure behaviors in rock and rock-like materials. *Theor Appl Fract Mec*. <https://doi.org/10.1016/j.tafmec.2023.103936>
- Lu XY, Qin RP, Dong CL, Fan CT (2023) Damage characteristics and energy evolution of bituminous sandstones under different cyclic amplitudes. *Appl Sci-Basel* 13(12):7340
- Lyu X, Yang K, Fang JJ (2022) Utilization of resources in abandoned coal mines for carbon neutrality. *Sci Total Environ*. <https://doi.org/10.1016/j.scitotenv.2022.153646>
- Lyu X, Yang K, Fang JJ, Tang JZ, Wang Y (2023a) Feasibility study of construction of pumped storage power station using abandoned mines: a case study of the shitai mine. *Energies* 16(1):314
- Lyu X, Yang K, Fang JJ, Duan MK, Wang Y, Zhang ZN (2023b) Experimental research and mechanism analysis of negative pressure grouting reinforcement of broken rock mass in goaf. *Chin J Rock Mech Eng* 42(S2):4174–4188
- Lyu X, Zhang T, Yuan L, Fang JJ (2023c) Prospects for the transformation and development of carbon storage in abandoned mines of coal enterprises from the perspective of carbon neutrality. *Int J Coal Sci Technol*. <https://doi.org/10.1007/s40789-023-00593-6>
- Ma DD, Wu Y, Yin JD, Lu JJ, Hu DW, Zhou H (2023a) Effect of initial pore pressure on the hydraulic fracturing of tight sandstone: an experimental study. *Geomech Geophys Geo*. <https://doi.org/10.1007/s40948-023-00547-x>
- Ma G, Chen X, Fan C, Ge S (2023b) Micro seepage characteristics and macro failure of coal under different hydraulic loading paths. *Rock Soil Mech* 44(6):1779–1788
- Ma JP, Zhang GC, Zhou GL, Zhang Y, Meng XJ, Zhao YQ, Chen M (2023c) Stability analysis of artificial dam in coal mine underground water reservoir based on the hydro-mechanical damage model. *Geomat Nat Haz Risk*. <https://doi.org/10.1080/19475705.2023.2190855>
- Maddu R, Pradhan I, Ahmadisharaf E, Singh SK, Shaik R (2022) Short-range reservoir inflow forecasting using hydrological and large-scale atmospheric circulation information. *J Hydrol*. <https://doi.org/10.1016/j.jhydrol.2022.128153>
- Meng QB, Liu JF, Huang BX, Zhang ZZ, Long JK, Wu JY (2023a) Experimental analysis of the height-diameter ratio effect of rock energy under uniaxial cyclic loading-unloading conditions. *B Eng Geol Environ*. <https://doi.org/10.1007/s10064-023-03305-1>
- Meng QB, Liu JF, Pu H, Huang BX, Zhang ZZ, Wu JY (2023b) Effects of cyclic loading and unloading rates on the energy evolution of rocks with different lithology. *Geomech Energy Envir*. <https://doi.org/10.1016/j.gete.2023.100455>
- Nie W, Li CX, Hu JW, Saffari P, Wang WS, Luo MH (2023) Spatial variation of physical and mechanical properties of tailings under different rainfall intensities and the interaction pattern. *Geomech Geophys Geo*. <https://doi.org/10.1007/s40948-023-00625-0>
- Ren CH, Yu J, Liu XY, Zhang ZQ, Cai YY (2022) Cyclic constitutive equations of rock with coupled damage induced by compaction and cracking. *Int J Min Sci Technol* 32(5):1153–1165
- Song ZY, Wu YF, Zhang Y, Yang Y, Yang Z (2023) Mechanical responses and acoustic emission behaviors of coal under compressive differential cyclic loading (dcl): a numerical study via 3d heterogeneous particle model. *Int J Coal Sci Technol*. <https://doi.org/10.1007/s40789-023-00589-2>
- Tang CJ, Yao QL, Chen T, Shan CH, Li J (2022) Effects of water content on mechanical failure behaviors of coal samples. *Geomech Geophys Geo*. <https://doi.org/10.1007/s40948-022-00382-6>
- Wang K, Li X, Huang Z, Zhao MJ (2021) Experimental study on acoustic emission and resistivity response of sandstone

- under constant amplitude cyclic loading. *Adv Mater Sci Eng*. <https://doi.org/10.1155/2021/6637200>
- Wang M, Xi X, Guo QF, Pan JL, Cai MF, Yang ST (2023a) Sulfate diffusion in coal pillar: experimental data and prediction model. *Int J Coal Sci*. <https://doi.org/10.1007/s40789-023-00575-8>
- Wang P, Guo Y, Cui GZ, Zhang N, Xu XL, Yu CH, Li AR, Kan JG (2023b) Cumulative damage and bearing capacity attenuation law of anchorage structure interface under cyclic loading and unloading. *Geomech Geophys Geo*. <https://doi.org/10.1007/s40948-023-00612-5>
- Wang PT, Qi ZW, Ma C, Cai MF (2023c) Anisotropic behavior of the seepage-stress coupling mechanical model of coal pillars of underground reservoirs. *Geomech Geophys Geo*. <https://doi.org/10.1007/s40948-023-00549-9>
- Wang RH, Wei C, Liu J, Li Z, Tan YH (2023d) Macro and micro characteristics of jointed sandstone under cyclic loading and unloading. *Chin J Rock Mech Eng* 42(4):810–820
- Xue XR, Zhang K, Chen WM, Deng KY (2021) Experimental investigation and viscoelastic-plastic model for sandstone under cyclic tensile stress. *Geomech Geophys Geo*. <https://doi.org/10.1007/s40948-021-00272-3>
- Yang XB, Han XX, Wang XY, Zhang ZP (2019) Effects of constant amplitude cyclic loading on the nonuniform deformation of sandstone specimens. *Adv Civ Eng*. <https://doi.org/10.1155/2019/6120435>
- Yang K, Fang JJ, Lyu X, Tang JZ, Liu WJ (2022a) Uniaxial compression tests on red sandstone specimens after different high-temperature processing and cooling time. *B Eng Geol Environ*. <https://doi.org/10.1007/s10064-022-02887-6>
- Yang K, Lyu X, Fang JJ, Liu S, Wei Z, Liu WJ (2022b) Mechanical properties and anchorage angle optimization of rock mass with a weak intercalated layer. *Ksce J Civ Eng* 26(3):1111–1122
- Yang K, Lyu X, Liu QJ, Yang YQ, Chi XL, Fang JJ, Fu Q, Wang Y, Zhang ZN (2022c) Experimental study on the instability characteristics of the coal pillar-artificial dam bonded body left behind in the abandoned mine. *J Min Saf Eng* 39(06):1071–1083
- Yang Q, Wang X, Nie R, Chen C, Chen Y, Xu F (2023) Characteristics of the cumulative plastic deformation and pore water pressure of saturated sand under cyclic intermittent loading. *Rock Soil Mech* 44(6):1671
- Zhang B, Ni W, Hao XQ, Li HQ, Shen YP (2023a) A study on the development and evolution of fractures in the coal pillar dams of underground reservoirs in coal mines and their optimum size. *Processes*. <https://doi.org/10.3390/pr11061677>
- Zhang BC, Liang YP, Zou QL, Ding LQ, Ran QC (2023b) Experimental investigation into the damage evolution of sandstone under decreasing-amplitude stress rates and its implications for coalbed methane exploitation. *Environ Earth Sci*. <https://doi.org/10.1007/s12665-023-10825-2>
- Zhang C, Wang XJ, Han PH, Bai QS, Chen JH (2023c) Failure analysis of residual coal pillar under the coupling of mining stress and water immersion in the goaf underground water reservoir. *Environ Earth Sci*. <https://doi.org/10.1007/s12665-023-10978-0>
- Zheng Z, Su H, Wang W, Wang ZC, Liu ZB, He BG, Mei GX (2023) A new hydro-mechanical coupling constitutive model for brittle rocks considering initial compaction, hardening and softening behaviors under complex stress states. *Geomech Geophys Geo*. <https://doi.org/10.1007/s40948-023-00607-2>
- Zhou YQ, Sheng Q, Fu XD, Ding HF (2023) The difference between the dynamic deformation properties of rock material under seismic load and cyclic loading: a case study on kobe wave. *Mech Time-Depend Mat* 27(2):401–426

**Publisher's Note** Springer Nature remains neutral with regard to jurisdictional claims in published maps and institutional affiliations.